Adaptively switched time stepping scheme for direct aeroacoustic computations

Lu, HsuehJui

Li, ChungGang

Tsubokura, Makoto

(Citation)
AIP Advances,12(3):035340

(Issue Date)
2022-03-01

(Resource Type)
journal article

(Version)
Version of Record

(URL)
https://hdl.handle.net/20.500.14094/90009192

AIP Advances

Adaptively switched time stepping scheme for direct aeroacoustic computations

Cite as: AIP Advances 12, 035340 (2022); https://doi.org/10.1063/5.0076657
Submitted: 27 October 2021 • Accepted: 01 March 2022 • Published Online: 18 March 2022

HsuehJui Lu, ChungGang Li and Makoto Tsubokura

Adaptively switched time stepping scheme for direct aeroacoustic computations

Cite as: AIP Advances 12, 035340 (2022); doi: 10.1063/5.0076657
Submitted: 27 October 2021 • Accepted: 1 March 2022 •
Published Online: 18 March 2022

HsuehJui Lu,[1,2,a] ChungGang Li,[1,2,b] and Makoto Tsubokura[1,2,c]

AFFILIATIONS

[1] Computational Fluid Dynamics Laboratory, Department of Computational Science, Graduate School of System Informatics, Kobe University, 1-1 Rokkodai, Nada-ku, Kobe 657-8501, Japan
[2] Complex Phenomena Unified Simulation Research Team, RIKEN, Advanced Institute for Computational Science, Kobe, Japan

[a] E-mail: lsray@stu.kobe-u.ac.jp
[b] Author to whom correspondence should be addressed: cgli@aquamarine.kobe-u.ac.jp. Tel.: +81-78-803-6680.
[c] E-mail: tsubo@tiger.kobe-u.ac.jp

ABSTRACT

The physical variables involved in a flow field are of very different scales to those of the aeroacoustic field within the flow. Thus, direct aeroacoustic computations (DACs) require extremely small time steps to capture the fluctuations in the aeroacoustic field and stabilize the numerical scheme. As a result, the computation time for DACs can be very long. This paper describes an implicit Adaptively Switched Time Stepping (ASTS) scheme that enables the use of larger time steps when solving DAC problems. ASTS is based on the adaptive selection of the time stepping scheme according to the value of the residual. Early in the iteration process, an artificial time term is used to afford larger time steps while ensuring that the numerical scheme remains stable. Once the residual is less than some preset reference value, the artificial time term is removed, thus eliminating the Newton linearization error. Simulation results show that ASTS can reduce the computational cost of DACs by a factor of more than eight while maintaining the required level of accuracy.

I. INTRODUCTION

Aeroacoustic phenomena have a wide range of applications, from engineering fields such as automotive aeroacoustics to our daily life through the human phonation system.[1] However, applying direct aeroacoustic computations (DACs) to computational aeroacoustics (CAA) remains challenging because the different scales of the acoustic and flow fields coexist in the same computational domain. As a result, highly accurate methods require very short time steps to capture the physical variables in the acoustic field.

The low levels of numerical dispersion and dissipation from the time scheme mean that, generally, an explicit method can be adopted for DACs. One of the most popular explicit techniques is the Runge–Kutta method. Yokoyama *et al.*[2] used a standard third-order-accurate Runge–Kutta method to simulate a cascade of flat plates. The acoustic resonance emitted from the cascade was captured, and the numerical results were found to be in good agreement with experimental measurements. To achieve higher accuracy and more efficient computations, several optimized Runge–Kutta methods have been proposed. For example, a modified Runge–Kutta coefficient can achieve high-accuracy CAA by minimizing the dispersion and dissipation in the Fourier space over a large range of frequencies for linear operators.[3–5] However, even with optimized Runge–Kutta methods, the Courant–Friedrichs–Lewy (CFL) condition restricts the time step, potentially resulting in very long computation times. Hence, it might not be appropriate to use explicit methods for practical applications.

Relatively few DACs use implicit methods because the larger numerical dissipation and dispersion result in lower accuracy. Martin and Candler[6] modified the source term for the data-parallel lower–upper relaxation method,[7] thus minimizing the dispersive errors. The linear wave equation for the propagation of a one-dimensional disturbance under the condition of 16 points per wave was used to validate the modified method, showing that the dispersive errors could be significantly reduced as long as the CFL number was less than 0.05; otherwise, the error from the iterative process

would cause further deterioration of the accuracy. In other words, the most important advantage of the implicit scheme, which is to afford a larger time step, cannot necessarily be used in CAA. To adopt a larger time step while retaining sufficient accuracy in an implicit scheme, Lian *et al.*[8] developed the solution-limited time stepping (SLTS) approach to accelerate the speed of convergence to the steady state. This approach uses the value of the residual as the criterion for the stability of the numerical scheme and, thus, for determining whether a larger CFL number should be adopted to accelerate the convergence speed. Their scheme was extended to transient state problems by introducing a dual time stepping technique.[9] However, this excellent idea cannot be applied to DAC problems because of the Newton linearization error[10] introduced by the artificial time term in the dual time stepping approach.

This paper describes an implicit time stepping scheme that minimizes the computational resources required for DAC problems. The idea of the proposed scheme is based on solution-limited time stepping, but the value of the residual is used to decide when the artificial time term can be eliminated in order to remove the Newton linearization error. By adaptively switching the governing equation between that with and without the artificial time term, the proposed Adaptively Switched Time Stepping (ASTS) scheme can use larger time steps while maintaining sufficient accuracy and stability for DAC problems. Simulation results show that ASTS allows CFL numbers up to 40 to be adopted in DAC problems. Additionally, to accelerate the time required to reach the quasi-steady state, an extremely large CFL number of up to 160 can be used to force the rapid development of the flow in the initial stages. After reaching the quasi-steady state, the time step gradually decreases to the target time step, which is better suited to DAC problems. This use of extremely large CFL numbers to quickly reach the quasi-steady state and larger CFL numbers for DAC problems means that the ASTS scheme is a promising tool for CAA studies.

II. GOVERNING EQUATIONS

The governing equation is the two-dimensional Navier–Stokes equation,

$$\frac{\partial U}{\partial t} + \frac{\partial F_1}{\partial x_1} + \frac{\partial F_2}{\partial x_2} = 0, \tag{1}$$

where U is the conservative form and F_i is the flux term. Denoting the density of the fluid by ρ, the quantities included in U and F_i are

$$U = \begin{pmatrix} \rho \\ \rho u_1 \\ \rho u_2 \\ \rho e \end{pmatrix} \tag{2}$$

and

$$F_i = \begin{pmatrix} \rho u_i \\ \rho u_i u_1 + P\delta_{i1} - \mu A_{i1} \\ \rho u_i u_2 + P\delta_{i2} - \mu A_{i2} \\ (\rho e + P)u_i - \mu A_{ij} u_j - k\dfrac{\partial T}{\partial x_i} \end{pmatrix}, \ \forall i = 1, 2, \tag{3}$$

where $A_{ij} = \partial u_i/\partial x_j + \partial u_j/\partial x_i - 2/3(\nabla \cdot u)\delta_{ij}$. The pressure P is given by the ideal gas equation

$$P = \rho RT. \tag{4}$$

The dynamic viscosity and thermal conductivity of the fluid at temperature T are based on Sutherland's law,

$$\mu(T) = \mu_0 \left(\frac{T}{T_0}\right)^{\frac{3}{2}} \frac{T_0 + 110}{T + 110}, \tag{5}$$

$$k(T) = \frac{\mu(T)\gamma R}{(\gamma - 1)\,\mathrm{Pr}}, \tag{6}$$

where $\rho_0 = 1.1842\ \mathrm{kg/m^3}$, $\mu_0 = 1.85 \times 10^{-5}\ \mathrm{N\,s/m^2}$, $T_0 = 298.06\ \mathrm{K}$, $\gamma = 1.4$, $R = 287\ \mathrm{J/kg}$, and the Prandtl number $Pr = 0.71$.

III. NUMERICAL METHOD

The dual time stepping method is applied to solve the Navier–Stokes formulation in Eq. (1). Thus, the governing equation becomes

$$\frac{\partial UP}{\partial \tau} + \frac{\partial U}{\partial t} + \frac{\partial F_1}{\partial x_1} + \frac{\partial F_2}{\partial x_2} = 0, \tag{7}$$

where U_p is the primitive form of $[P,\ u_1,\ u_2,\ T]$. τ and t are, respectively, the artificial and physical time, and U is the conservative form of $[\rho,\ \rho u_1,\ \rho u_2,\ \rho e]$. $\partial U_p/\partial \tau$ is the artificial time term for the dual time stepping method to calculate the iteration during each real-time step. While the term of artificial time $\partial U_p/\partial \tau$ is convergent to zero, the real-time counts a proceeding step. Thereby, Eq. (7) automatically transfers into the original Navier–Stokes equation.

The discretized form of Eq. (7) is

$$\frac{\overline{U}_p^{k+1} - \overline{U}_p^{k}}{\Delta\tau} + \frac{3\overline{U}^{k+1} - 4\overline{U}^{n} + \overline{U}^{n-1}}{2\Delta t} + \frac{1}{\Delta x_1}\left(\overline{F}^{k+1}_{1(i+1/2,j)} - \overline{F}^{k+1}_{1(i-1/2,j)}\right) + \frac{1}{\Delta x_2}\left(\overline{F}^{k+2}_{2(i,j+1/2,j)} - \overline{F}^{k+1}_{2(i,j-1/2)}\right) = 0. \tag{8}$$

The superscripts k and n indicate the iteration numbers of artificial time and the preceding step of real time, respectively. When the artificial time term $\partial U_p/\partial \tau$ converges to zero, the quantities of the $(k+1)$th iteration in the artificial time term are approximately transferred to the quantities of the $(n+1)$th time step in real time.

Afterward, the terms of $\overline{U}^{K+1}$ and $\overline{F}_i^{K+1}$ in Eq. (8) are necessary to be linearized and expressed, respectively, as follows:

$$\overline{U}^{K+1} = \overline{U}^{K} + M\Delta\overline{U}_p, \tag{9}$$

where $M = \partial\overline{U}/\partial\overline{U}_p$ and $\Delta\overline{U}_p = \overline{U}_p^{\,k+1} - \overline{U}_p^{\,k}$,

$$\overline{F}_i^{\,K+1} = \overline{F}_1^{\,K} + A_p\Delta\overline{U}_p, \tag{10}$$

where $A_p = \partial\overline{F}_1^{\,k}/\partial\overline{U}_p$ is the flux Jacobian and the same methods of $B_p = \partial\overline{F}_2^{\,k}/\partial\overline{U}_p$ are used in linearization of $\overline{F}_2^{\,K+1}$.

Substituting Eqs. (9) and (10) into Eq. (8), the following equation is obtained:

$$\frac{\Delta\overline{U}_p}{\Delta\tau}+\frac{3(\overline{U}^k+M\Delta\overline{U}_p)-4\overline{U}^n+\overline{U}^{n-1}}{2\Delta t}+\frac{1}{\Delta x_1}(\overline{F}_1{}^k+A_p\Delta\overline{U}_p)+\frac{1}{\Delta x_2}(\overline{F}_2{}^k+B_p\Delta\overline{U}_p)=0. \tag{11}$$

Equation (11) can be rearranged as

$$\left[M^{-1}\frac{I}{\Delta\tau}+\frac{3}{2\Delta t}+M^{-1}\left(\delta_{x_1}A_p^k+\delta_{x_2}B_p^k\right)\right]\Delta U_p=M^{-1}R^k, \tag{12}$$

where $M=\partial U/\partial U_p$, δ_{x_i} is the central-difference operator, I is the unit matrix, and $R^k=-\left(3U^k-4U^n+U^{n-1}\right)/(2\Delta t)-\left(\delta_{x_1}\overline{F}_1^k+\delta_{x_2}\overline{F}_2^k\right)$.

In the computation of R^n on the right-hand side of Eq. (12), the terms involving F_i in Eq. (3) can be divided into two parts. One is the inviscid term $F_{inviscid}$, expressed as

$$F_{inviscid}=\begin{pmatrix}\rho u_i\\ \rho u_i u_1+P\delta_{i1}\\ \rho u_i u_2+P\delta_{i2}\\ (\rho e+P)u_i\end{pmatrix}, \tag{13}$$

and the other is the viscous term $F_{viscous}$, expressed as

$$F_{viscous}=-\begin{pmatrix}0\\ \mu A_{i1}\\ \mu A_{i2}\\ \mu A_{ij}u_j+\lambda\dfrac{\partial T}{\partial x_i}\end{pmatrix}. \tag{14}$$

To obtain more accurate results at low Mach numbers, Eq. (13) is solved using the low-Mach-fix for Roe (LMRoe) method,[11] whereby

$$F_{inviscid,i+1/2}=\frac{1}{2}(F_R+F_L)+F_d, \tag{15}$$

where F_d is the Roe upwind dissipation term given by

$$F_d=-\frac{1}{2}\left\{|U|\begin{bmatrix}\Delta\rho\\ \Delta(\rho u)\\ \Delta(\rho v)\\ \Delta(\rho E)\end{bmatrix}+\delta U\begin{bmatrix}\rho\\ \rho u\\ \rho v\\ \rho H\end{bmatrix}+\delta\begin{bmatrix}0\\ 1\\ 0\\ u\end{bmatrix}\right\}, \tag{16}$$

and

$$\delta U=(c-|u|)\frac{\Delta p}{\rho c^2}+\frac{u}{c}f(M)\Delta\frac{1}{2}u, \tag{17}$$

where $f(M)=(|u|+|v|+|w|)/c$, and

$$\delta p=\frac{u}{c}\Delta p+\left(c'-|u|\right)\rho\Delta u,\quad c'=f(M)c. \tag{18}$$

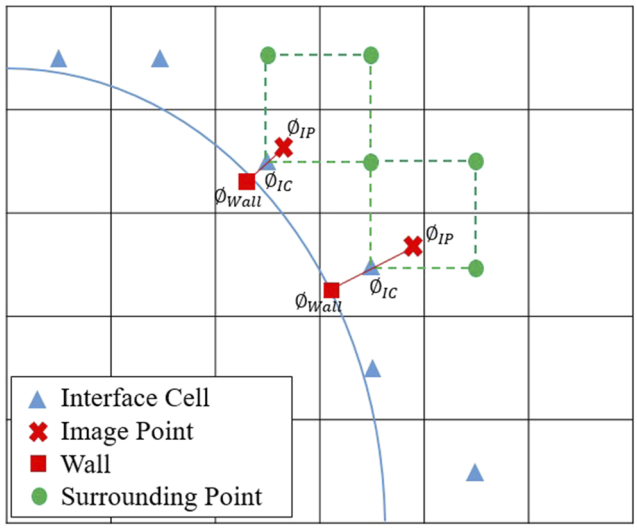

FIG. 1. Compressible immersed boundary method configuration.

To calculate F_R and F_L in Eq. (15), the fifth-order monotone upstream-centered scheme for conservation laws (MUSCL)[12] with no limiter function is adopted. The fifth-order MUSCL without a limiter function can be written as

$$U^L_{i+1/2}=1/6\times(2U_{i-2}+13U_{i-1}+47U_i+27U_{i+1}+3U_{i+2}), \tag{19}$$

$$U^R_{i-1/2}=1/6\times(-3U_{i-2}+27U_{i-1}+47U_i-13U_{i+1}+2U_{i+2}). \tag{20}$$

In addition to the inviscid term, the derivatives of A_{ij} in the viscous term of Eq. (14) are computed using the second-order central difference.

As boundary conditions on the wall, a no-slip condition is imposed on the velocity and a zero-gradient is applied in the normal direction for the pressure and density using the immersed boundary method (IBM) for compressible flow.[13] The configuration is shown in Fig. 1. The IBM can be summarized in the following steps: (i) The interface cell (IC) is defined by calculating the distance between the wall and the center of the cell within a range of one cell. (ii) The image point (IP) is defined as the point at which the distance between the IP and IC is equal to the distance between the IC and the wall in the normal direction. (iii) The value of the IP can be interpolated using the surrounding points, and the value of IC can be interpolated using the IP and the wall value. Thus, the IP and IC are coupled. (iv) By solving the coupled equation, Dirichlet or Neumann boundary conditions can be imposed. The whole framework is based on a hierarchal structure system named CUBE (for more detailed information, refer to Refs. 14 and 15). Absorbing and non-reflecting boundary conditions[16] are adopted at the outermost boundary to prevent reflections from affecting the results.

IV. ADAPTIVELY SWITCHED TIME STEPPING SCHEME

To set the artificial time step $\Delta\tau$ in Eq. (12) so as to accelerate the convergence speed, Lian *et al.*[8] proposed the brilliant solution-limited time stepping (SLTS) method. This was employed alongside

the lower–upper symmetric Gauss–Seidel (LUSGS) implicit method to adaptively adjust the CFL number and determine $\Delta\tau$.

When adopting LUSGS to solve Eq. (12), the estimation value ΔQ_{est}, which is defined in Eq. (21), provides a criterion for determining whether the calculation is stable or not,[8]

$$\Delta Q_{est} = -\Delta\tau M^{-1}\left[-\left(3U^k - 4U^n + U^{n-1}\right)/(2\Delta t) - \left(\delta_{x_1}\overline{F}_1^k + \delta_{x_2}\overline{F}_2^k\right)\right]. \tag{21}$$

According to the numerical test in Ref. 8, if any component of ΔQ_{est} is less than the reference value ΔQ_{ref} defined in Eq. (22), the calculation is stable. Hence, the CFL number based on the artificial time step $\Delta\tau$ can be increased to accelerate the speed of convergence. In this situation, CFL is set to some value $CFL_{specified}$, which has a recommended value of 1000,[8]

$$\Delta Q_{ref} = \begin{pmatrix} \alpha_1 \times \max\left[0.5 \times \rho\left(u_1^2 + u_2^2\right), \quad \Delta P_{sur}, \quad P_{global} \times 10^{-9}\right] \\ \alpha_2 \times \max\left[\left(u_1^2 + u_2^2\right), \quad \dfrac{\Delta P_{sur} \times c}{\gamma P} \quad V_{global} \times 10^{-9}\right] \\ \alpha_3 \times \max\left[\left(u_1^2 + u_2^2\right), \quad \dfrac{\Delta P_{sur} \times c}{\gamma P} \quad V_{global} \times 10^{-9}\right] \\ \alpha_4 \times T \end{pmatrix}, \tag{22}$$

where ΔP_{sur} is the maximum difference between the pressure at surrounding points and P_{global}, V_{global} denotes some global value that ensures the reference values are always greater than 0, c is the speed of sound, and γ is the heat capacity ratio. $\begin{bmatrix} \alpha_1 & \alpha_2 & \alpha_3 & \alpha_4 \end{bmatrix}$ is the coefficient of the maximum allowable fractional change, which has a suggested value of $\begin{bmatrix} 0.1 & 2 & 2 & 0.1 \end{bmatrix}$.[8]

If any one component of ΔQ_{est} is greater than ΔQ_{ref}, the calculation is not stable, and the CFL number should be decreased to prevent the calculation from diverging. Equation (20) is used to decrease the CFL number appropriately,

$$CFL_{allowable} = CFL_{specified} \times \alpha \times \Delta Q_{residual}/|\Delta Q_{est}|, \tag{23}$$

where a value of $\alpha = 0.2$ has been used in previous studies.[8] $CFL_{allowable}$ is then adopted as the artificial time step.

Under the SLTS method, the maximum allowable CFL number is automatically evaluated, and the maximum allowable artificial time step $\Delta\tau$ can be determined to accelerate the speed of convergence. Additionally, the value of the physical time step is not restricted by the CFL condition because of the dual time stepping. Overall, a larger physical time step and faster speed of convergence can be achieved, thus drastically reducing the computational resources required.

However, SLTS is not suitable for aeroacoustic simulations because the Newton linearization error of the term $\partial U_p/\partial\tau$ persists, even when the convergence criteria are satisfied. This kind of small error will destroy the accuracy of the acoustic field because physical values in the acoustic field are usually 2–3 orders of magnitude smaller than those in the flow field.

A straightforward method of removing the Newton linearization error was suggested by Xu *et al.*[10] They found that the term containing the artificial time term, $M^{-1}I/\Delta\tau$, can be set to zero in Eq. (12). This drives the Newton linearization error to zero, leaving

$$\left[\frac{3}{2\Delta t} + M^{-1}\left(\delta_{x_1}A_p^k + \delta_{x_2}B_p^k\right)\right]\Delta U_p = M^{-1}R^k. \tag{24}$$

In this situation, the artificial time step is effectively set to infinity in Eq. (12), significantly increasing the convergence speed.

TABLE I. Computational parameters of flow-induced noise around a cylinder.

Time step (s)	3.26×10^{-8}; 6.52×10^{-8}; 1.30×10^{-7}; 2.61×10^{-7}
CFL number	20; 40; 80; 160
Total number of cubes N_{cube}	16 186
Cell number in a cube	16 × 16 (2-dimensional)
Total number of cells N_{cell}	4 143 616
Size of the largest cell SL_{cell} (mm)	0.0216
Size of the smallest cell SS_{cell} (mm)	6.75×10^{-4}
Computational domain $X_1 \times X_2$ (mm^3)	11.0592 × 11.0592
Inlet velocity U (m/s)	69
Dimensionless pressure (Pa) $\rho_0 c^2$	1.4182×10^5
Cylinder diameter D (mm)	0.045
Reynolds number	200

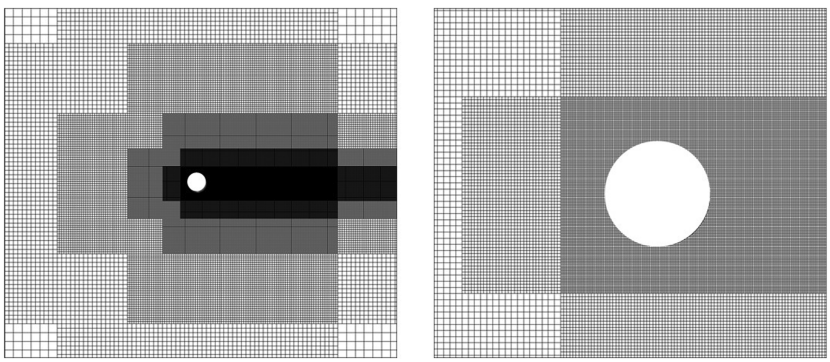

(a) (b)

FIG. 2. (a) Grid distribution around the cylinder. (b) Magnified view of the grid distribution.

TABLE II. Comparison of results with CFL = 20, 40, 80, and 160.

	CFL number	Drag coefficient C_D	Lift coefficient C_L	Strouhal number St
CFL = 20	20	1.40 (2.2%)	0.69 (1.4%)	0.201 (1.0%)
CFL = 40	40	1.41 (2.9%)	0.71 (1.4%)	0.193 (1.3%)
CFL = 80	80	1.46 (6.6%)	0.81 (15.7%)	0.170 (14.6%)
CFL = 160	160	1.50 (9.5%)	0.87 (24.3%)	0.118 (40.7%)
Reference 17		1.37	0.7	0.199 (2.2%)

However, Eq. (24) cannot accommodate such a large physical time step because of the lack of the artificial time term. Therefore, to adopt a larger physical time step while still avoiding the Newton linearization error, we propose the Adaptively Switched Time Stepping (ASTS) scheme.

Inside the iteration process, when ΔQ_{est} is greater than ΔQ_{ref}, the numerical scheme is not yet stable, and so the whole framework is the same as SLTS, which means Eq. (23) is used to obtain the artificial time step for solving Eq. (12). Once ΔQ_{est} is less than ΔQ_{ref}, however, Eq. (24) can be applied to remove the Newton linearization error because the numerical scheme is already stable.

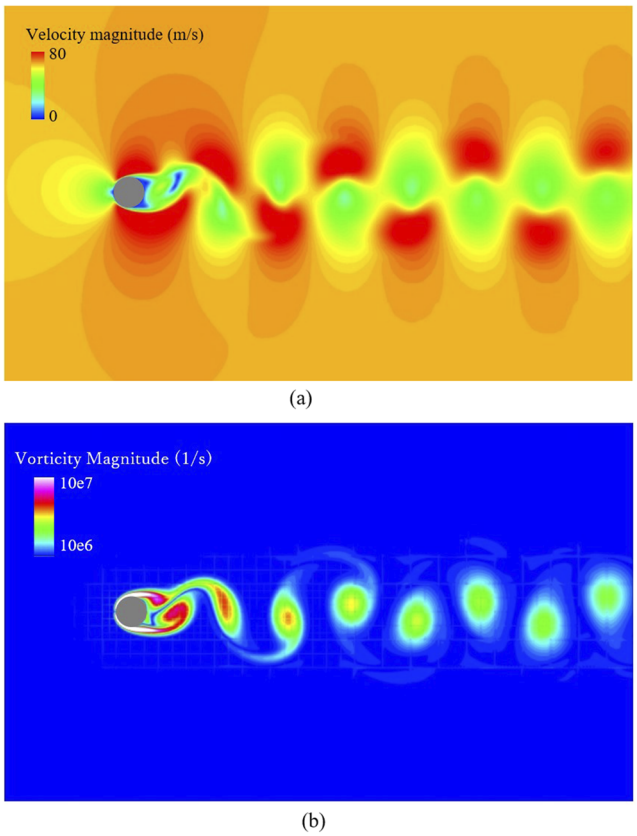

FIG. 3. Instantaneous velocity field and Karman vortex shedding. (a) Contours of velocity magnitude. (b) Contours of vorticity magnitude.

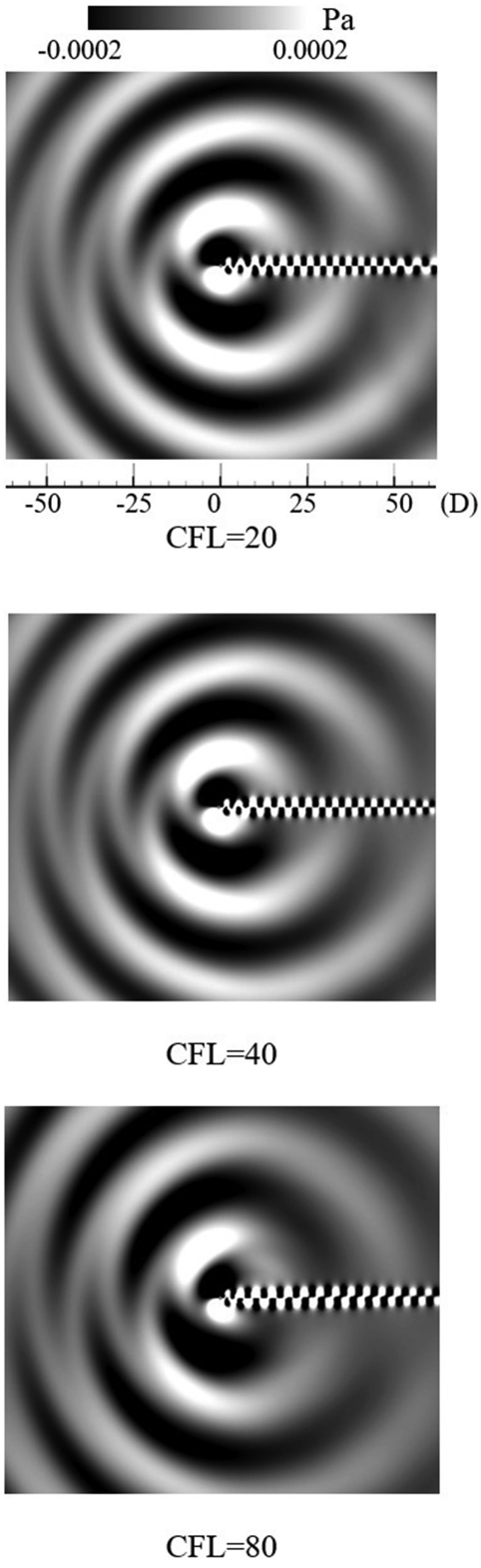

FIG. 4. Comparison of the contours of instantaneous pressure fluctuations.

The solution procedures of ASTS can be briefly summarized in the following two steps:

1. Calculate Eqs. (18) and (19) to obtain the values of ΔQ_{est} and ΔQ_{ref}, respectively.
2. If $\Delta Q_{est} > \Delta Q_{ref}$, use Eq. (23) to calculate $\Delta\tau$ and solve Eq. (12); if $\Delta Q_{est} < \Delta Q_{ref}$, solve Eq. (24) directly.

When performing the implicit time stepping scheme, the initial guess for the iteration is usually the result of the current time step, which means we set $U^{k+1,k=0} - U^n$ for R_k in Eq. (12). After N_k iterations, $U^{k+1,k=N_k}$ approaches U^{n+1}, i.e., the iteration process has converged, and we move to the next physical time step. For ASTS, Eq. (12) is first applied until $\Delta Q_{est} < \Delta Q_{ref}$, whereupon Eq. (24) is used. Hence, the initial guess for Eq. (24) is actually the SLTS result after several iterations, which means the initial guess for Eq. (24) in ASTS is already an approximation of U^{n+1}. This is why Eq. (24) can use a larger time step while retaining sufficient accuracy.

V. RESULTS AND DISCUSSION

The proposed ASTS scheme was validated by simulating and capturing the tonal noise generated by a laminar flow passing a two-dimensional circular cylinder at Re = 200 with a free stream velocity of Mach 0.2. The resulting aerodynamic properties, such as the drag coefficient, lift coefficient, and Strouhal number, were then compared with those reported by Linnick and Fasel,[17] whereas the properties of the acoustic field, such as the pressure fluctuations, were compared with those presented by Seo and Mittal.[18]

The computational parameters are listed in Table I, and the grid distribution is shown in Fig. 2. The immersed boundary method with the cube grid divided according to the hierarchical structure system proposed by Nakahashi and Kim[14] was applied for the grid spacing. The finest mesh around the cylinder and its wake is around 0.015D, where D is the diameter, while far from the cylinder, a much coarser resolution of around 0.48D is adopted. According to Ref. 18, the wavelength in the far field is around 25D, where a sufficient resolution of around 50 points per wave can be ensured in the present simulations. Additionally, an absorbing, non-reflecting boundary[16] is adopted at the outermost cubes.

Using the proposed ASTS scheme, simulations were conducted with four different CFL numbers (20, 40, 80, and 160, based on sound speed plus the inlet speed). The number of inner iterations was set to 100 to ensure a fair evaluation of the computation time. For explicit methods, the CFL number should generally be less than 1 to ensure that the numerical scheme is stable. For implicit methods, the CFL number is typically less than 10 to guarantee accurate results. The proposed scheme can use larger time steps that imply a CFL number above 20. The simulation results are summarized in Table II.

For the case of CFL = 20, Fig. 3 shows the instantaneous velocity field. Karman vortex shedding in the wake region can be clearly observed. Additionally, the drag coefficient, lift coefficient, and Strouhal number are in good agreement with the results presented in Ref. 17. Based on the results with CFL = 20, it is clear that ASTS not only allows a larger CFL number but also obtains accurate results in terms of the aerodynamic properties.

As the CFL number increases, the discrepancies with respect to the results in Ref. 17 become larger. When CFL = 40, the drag coefficient and the Strouhal number are slightly overestimated, but the error is within 3%. Once the CFL number is greater than 80, the discrepancies in both the lift coefficient and the Strouhal number are greater than 10%. Overall, when the CFL number is less than 40, ASTS can still obtain accurate results.

Figure 4 shows the instantaneous pressure fluctuation, which is given by

$$P' = \frac{P - \overline{P}}{\rho_0 c^2}, \tag{25}$$

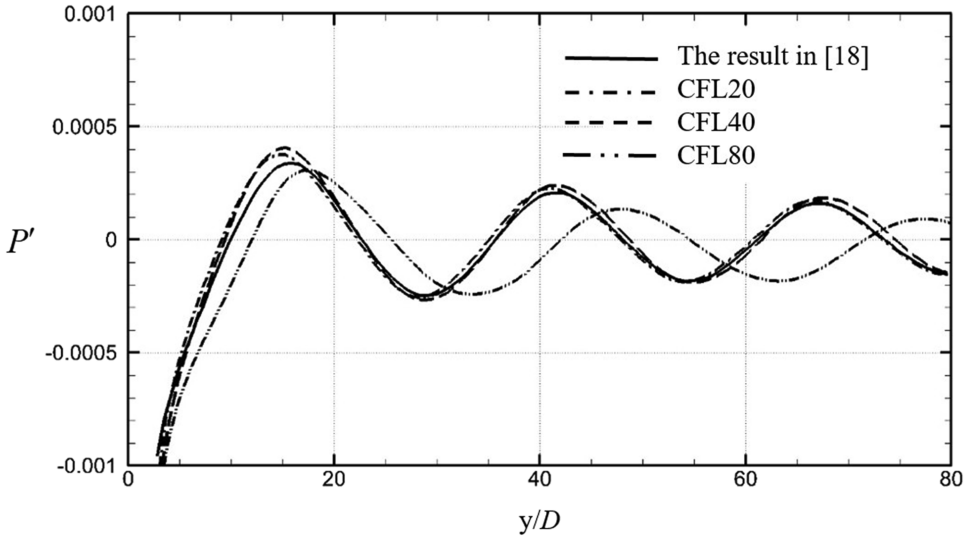

FIG. 5. Comparison of instantaneous pressure fluctuations with the results in Ref. 18.

where $\overline{P}$ is the time-averaged pressure field, ρ_0 is the ambient density, and c is the speed of sound. For CFL = 20 and CFL = 40, the acoustic field presented in the figure compares well with the corresponding field reported by Ref. 18. The propagation of pressure fluctuations from the cylinder to the far field can be observed, and the vortex sound source behind the cylinder can be identified. For the case of CFL = 80, the enhanced numerical dissipation caused by the large time step degrades the shape of the wave, especially near the vortex sound source, which changes the wavelength of the propagation.

The instantaneous pressure fluctuations along the line x = 0 above the cylinder are compared in Fig. 5. Note the extremely small scale of the pressure fluctuations, which are ~0.01% of the dominant pressure, $\rho_0 c^2$. A highly accurate scheme is required to capture such small-scale phenomena. For the case of CFL = 20 and CFL = 40, the distribution is highly consistent with that reported in Ref. 17. However, for CFL = 80, the amplitude is underestimated, while the wavelength is overestimated.

From the above results, it can be concluded that ASTS not only enhances the computational efficiency by enabling a larger time step but also obtains accurate results. It has been shown that ASTS can be applied to acoustic problems. Increasing the time step to

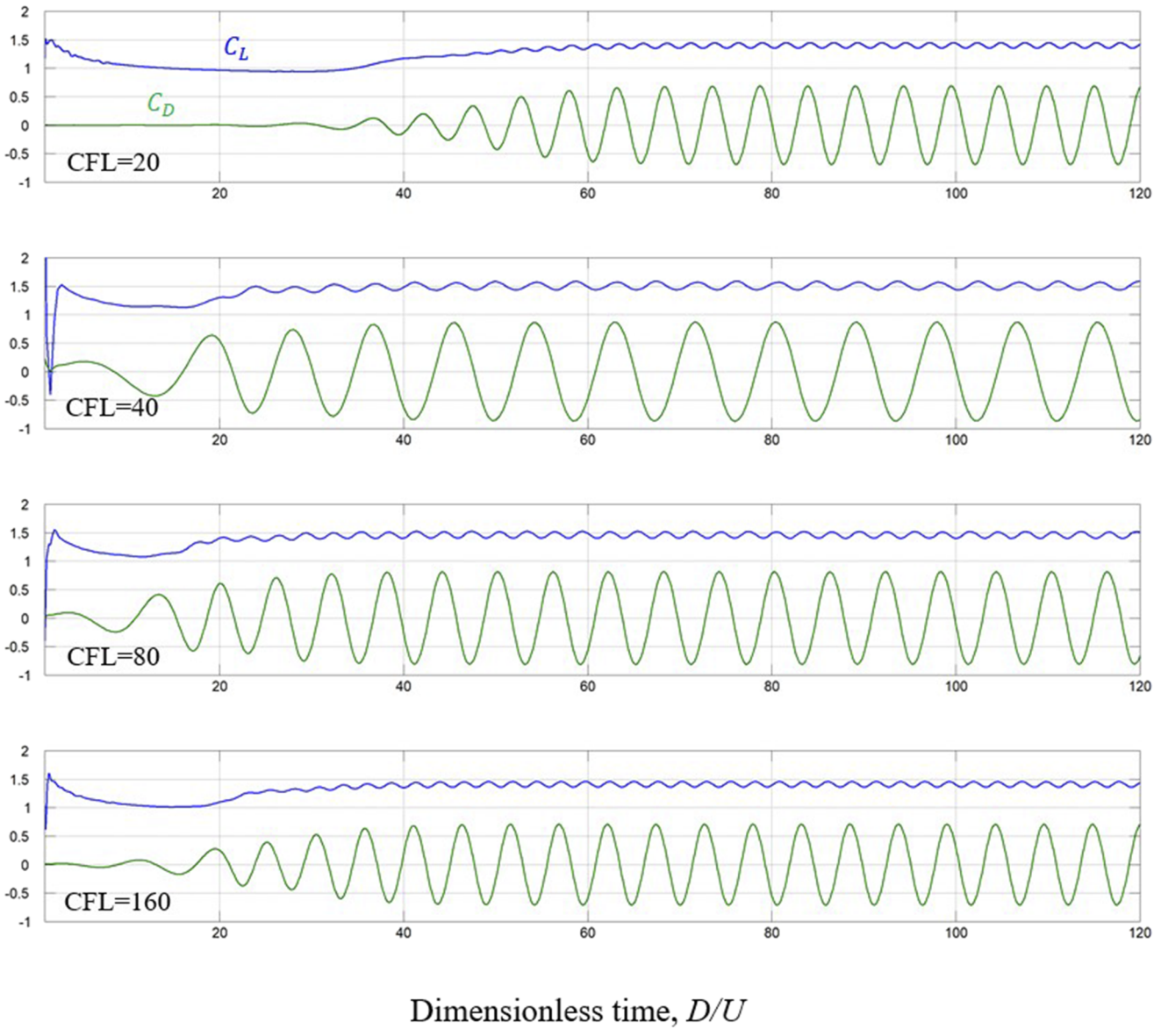

FIG. 6. Drag coefficients C_D and lift coefficients C_L with respect to dimensionless time.

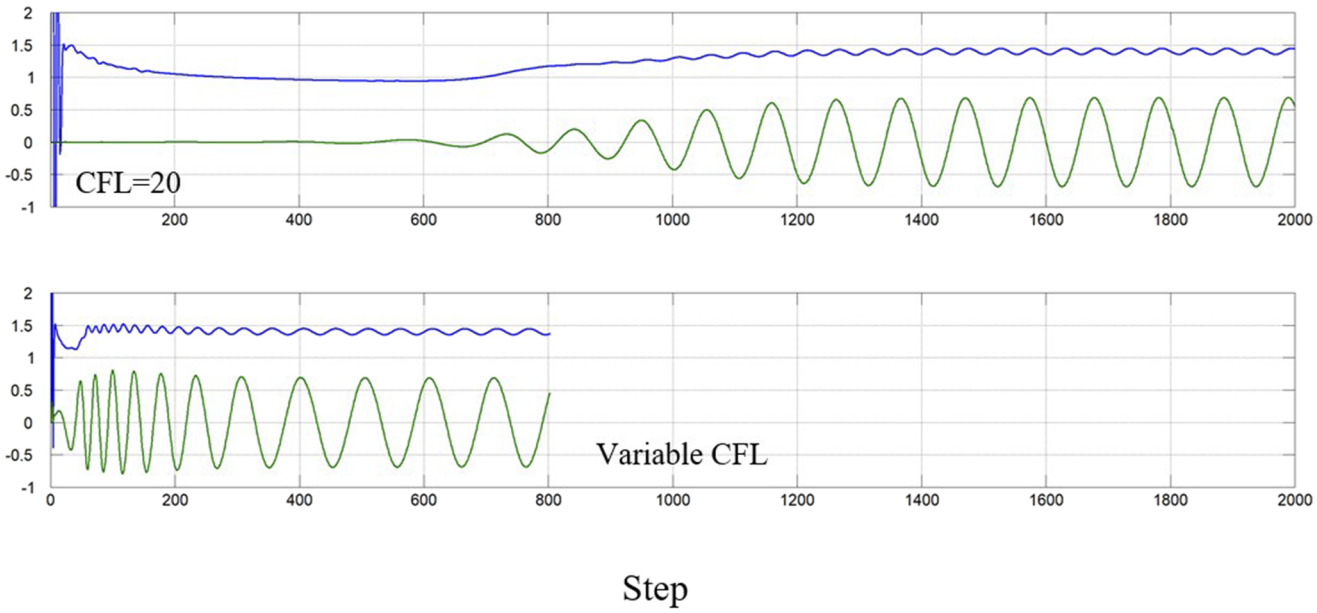

FIG. 7. Comparison of time required to reach the quasi-steady state between constant and variable steps.

accelerate the time required to reach the quasi-steady state, ASTS provides a robust method for adjusting both the calculation time and the accuracy.

Figure 6 shows the history of the drag and lift coefficients with respect to (dimensionless) time (D/U) for four cases. Although CFL = 80 and CFL = 160 produce inaccurate results as the time steps are excessively large, they reach the quasi-steady state much faster than when CFL = 20. Therefore, an idea is proposed here. In the early stages, the development of the flow field can be accelerated by adopting an excessively large time step. Once the flow field reaches the quasi-steady state, the time step is gradually decreased to an appropriate value for ensuring accurate results. An example is provided in Fig. 7, which shows the history of the drag and lift coefficients with CFL = 20 and with a variable time step. For CFL = 20, the time step is constant, and ~1200 iterations are required to reach the quasi-steady state. In the case with variable time steps, CFL = 160 is adopted in the early stages, and then the time step is gradually decreased with a decay coefficient of 0.9 until CFL is less than 20. This decay process takes only another 20 steps $\left(160 \times 0.9^{20} = 19.45\right)$. Finally, another 200 steps are required until the flow is fully developed. In total, fewer than 300 iterations are required to reach the quasi-steady state. Compared with CFL = 20 and a constant time step, this represents a reduction of over 75% in terms of the computation time, although the level of accuracy remains unchanged. Compared with the traditional LUSGS implicit scheme, where the CFL number is typically less than 10 for transient state problems, the computation time of the proposed ASTS method is up to eight times faster (four times faster with the variable time steps and twice as fast with larger time steps). This is because the calculation of Eq. (21), which is also needed for the traditional LUSGS, and Eq. (22) can be almost neglected.

VI. CONCLUSION

A new implicit time scheme based on the SLTS and LUSGS schemes has been developed for DAC problems. In the proposed ASTS scheme, the residual term is used as an indicator for adaptively determining whether the governing equation includes an artificial time step or not, thus eliminating the Newton linearization error. Simulation results show that when the CFL number is less than 40, acceptable accuracy can be achieved in both aerodynamic and aeroacoustic problems. Additionally, larger time steps reduce the calculation time. Therefore, in the early stages, larger time steps are used to quickly develop the flow, and then the time step is gradually decreased to ensure accurate results. This approach significantly reduces the computation time. According to our results, the computation time can be reduced by a factor of eight compared with the traditional LUSGS. Therefore, the proposed ASTS scheme has the advantages of high efficiency, high accuracy, and widespread applicability for both fluid and acoustic calculations.

ACKNOWLEDGMENTS

This work was supported by RIKEN Junior Research Associate Program and JST CREST Grant Number JPMJCR20H7, Japan.

AUTHOR DECLARATIONS

Conflict of Interest

The authors have no conflicts to disclose.

DATA AVAILABILITY

The data that support the findings of this study are available from the corresponding author upon reasonable request.

NOMENCLATURE

ASTS	adaptively switched time stepping
CAA	computational aeroacoustics
CFL	Courant–Friedrichs–Lewy
DAC	direct aeroacoustic computations
IBM	immersed boundary method
IC	interface cell
IP	image point
LUSGS	lower–upper symmetric Gauss–Seidel
MUSCL	monotone upstream-centered scheme for conservation laws
Pr	Prandtl number
SLTS	solution-limited time stepping
St	Strouhal number

REFERENCES

[1]T. Yoshinaga, K. Nozaki, and S. Wada, "Experimental and numerical investigation of the sound generation mechanisms of sibilant fricatives using a simplified vocal tract model," Phys. Fluids **30**, 035104 (2018).
[2]H. Yokoyama, K. Kitamiya, and A. Iida, "Flows around a cascade of flat plates with acoustic resonance," Phys. Fluids **25**, 106104 (2013).
[3]F. Q. Hu, M. Y. Hussaini, and J. L. Manthey, "Low-dissipation and low-dispersion Runge–Kutta schemes for computational acoustics," J. Comput. Phys. **124**, 177–191 (1996).
[4]C. Bogey and C. Bailly, "A family of low dispersive and low dissipative explicit schemes for flow and noise computations," J. Comput. Phys. **194**, 194–214 (2004).
[5]J. Berland, C. Bogey, and C. Bailly, "Low-dissipation and low-dispersion fourth-order Runge–Kutta algorithm," Comput. Fluids **35**, 1459–1463 (2006).
[6]M. P. Martín and G. V. Candler, "A parallel implicit method for the direct numerical simulation of wall-bounded compressible turbulence," J. Comput. Phys. **215**, 153–171 (2006).
[7]G. V. Candler, M. J. Wright, and J. D. McDonald, "Data-parallel lower-upper relaxation method for reacting flows," AIAA J. **32**, 2380–2386 (1994).
[8]C. Lian, G. Xia, and C. L. Merkle, "Solution-limited time stepping to enhance reliability in CFD applications," J. Comput. Phys. **228**, 4836–4857 (2009).
[9]C. Lian, G. Xia, and C. L. Merkle, "Impact of source terms on reliability of CFD algorithms," Comput. Fluids **39**, 1909–1922 (2010).
[10]X. Xu, J. S. Lee, and R. H. Pletcher, "A compressible finite volume formulation for large eddy simulation of turbulent pipe flows at low Mach number in Cartesian coordinates," J. Comput. Phys. **203**, 22–48 (2005).
[11]F. Rieper, "A low-Mach number fix for Roe[R8S2Q1M7]s approximate Riemann solver," J. Comput. Phys. **230**, 5263–5287 (2011).
[12]K. H. Kim and C. Kim, "Accurate, efficient and monotonic numerical methods for multi-dimensional compressible flows part II: Multi-dimensional limiting process," J. Comput. Phys. **208**, 570–615 (2005).
[13]C.-G. Li, M. Tsubokura, and R. Bale, "Framework for simulation of natural convection in practical applications," Int. Commun. Heat Mass Transfer **75**, 52–58 (2016).
[14]K. Nakahashi and L. Kim, "Building-cube method for large-scale, high resolution flow computations," in *42nd AIAA Aerospace Sciences Meeting and Exhibit* (AIAA, 2004), pp. 1–9.
[15]N. Jansson, R. Bale, K. Onishi, and M. Tsubokura, "CUBE: A scalable framework for large-scale industrial simulations," Int. J. High Perform. Comput. Appl. **33**, 678 (2018).
[16]C.-G. Li, M. Tsubokura, W.-S. Fu, N. Jansson, and W.-H. Wang, "Compressible direct numerical simulation with a hybrid boundary condition of transitional phenomena in natural convection," Int. J. Heat Mass Transfer **90**, 654–664 (2015).
[17]M. N. Linnick and H. F. Fasel, "A high-order immersed interface method for simulating unsteady incompressible flows on irregular domains," J. Comput. Phys. **204**, 157–192 (2005).
[18]J. H. Seo and R. Mittal, "A high-order immersed boundary method for acoustic wave scattering and low-Mach number flow-induced sound in complex geometries," J. Comput. Phys. **230**, 1000–1019 (2011).